International Journal of Chemical Science
Online ISSN: 2523-2843, Print ISSN: 2523-6075; Impact Factor: RJIF 5.22
Received: 02-01-2020; Accepted: 03-02-2020; Published: 13-02-2020
www.chemicaljournals.com
Volume 4; Issue 1; 2020; Page No. 09-16

The change of phase states in situ of the charge carriers toward the high H_2 performance of Cu_2O/TiO_2 nanocomposite via p-n heterojunction

Le Thi Ngoc Tu[1*], Ton Nu Quynh Trang[2], Vu Thi Hanh Thu[3]
[1] Falculty of Physics, Dong Thap University, Vietnam
[2, 3] Falcuty of Physics and Engineering Physics, University of Science, Vietnam

Abstract
The charge carriers in the heterojunction structure are playing a significant role in the photocatalytic toward hydrogen evolution reaction. Herein, we focus on analyzing the change of the influence of annealing treatment upon the structural properties and the photocatalytic hydrogen performance of Cu_2O/TiO_2 heterojunction structure. Our results show that the efficiency and the rate of photocatalytic hydrogen generation over the Cu_2O/TiO_2 samples were found to be higher than TiO_2 owing to the occurrence of the charge carrier transport via p-n heterojunction between Cu_2O and TiO_2 that can be suppressed the recombination rate of photogenerated electron-hole pairs. Moreover, after being annealed the various temperatures from 300°C-700°C, the obtained H_2 evolution of Cu-based photocatalyst significantly affected due to the presence of transition phase from anatase to rutile in the crystal structure, leading to the change the redox potential in heterojunction. It is noticed that the highest hydrogen of the CuO/TiO_2-500 photocatalyst with an apparent quantum yield of about 10.8% was obtained compared with others under the same conditions. These results will provide insight for clean energy evolution in the future based on the p-n heterojunction structure.

Keywords: nanostructures, semiconductors, hydrothermal, catalytic properties, hydrogen production

1. Introduction
Using the semiconductor play as the photocatalyst for hydrogen (H_2) production from photocatalytic water-splitting is a helpful way for clean energy, environmentally friendly, and cost-effective. Due to the smallest voltage required for water splitting reaction is the minimum energy of 1.23 eV to convert water into H_2 and O_2. This is equated to change in Gibb's free energy ΔG_o = + 237.2 kJ/mol or an equivalent of 1.23 V [1, 2]. Therefore, using a semiconductor as a photocatalytic to generate H_2 gas, they need have some properties as follows: i) their bandgap energy must be large enough to spilt water (E_g > 1.23 V); ii) the redox potential of conduction band-edge energy (CB) and valence band-edge energy (VB) have more suitable for the electrochemical potentials $E°(H^+/H_2)$ and $E°(O_2/H_2O)$. These factors can drive the hydrogen evolution reaction and the oxygen evolution reaction using electron-hole pairs generated under irradiation light [3].
In various semiconductors, TiO_2 is considered as a good photocatalyst for the H_2 generation due to its strong oxidation-reduction ability under light irradiation, nontoxicity, stable, environmentally friendly, abundant, and low-priced. More importantly, the CB and VB energy levels of TiO_2 are suitable for the photocatalytic water splitting reactions (Fig. 1) [4]. The VB of TiO_2 is more positive than the oxidation energy level of water and the CB of TiO_2 is more negative than the reduced energy level of water [3], therefore, TiO_2 is an applicable choice for photocatalytic hydrogen generation from water splitting process under solar irradiation. Their position of the band edges for the water splitting to produce the H_2 can be described in Fig. 1.

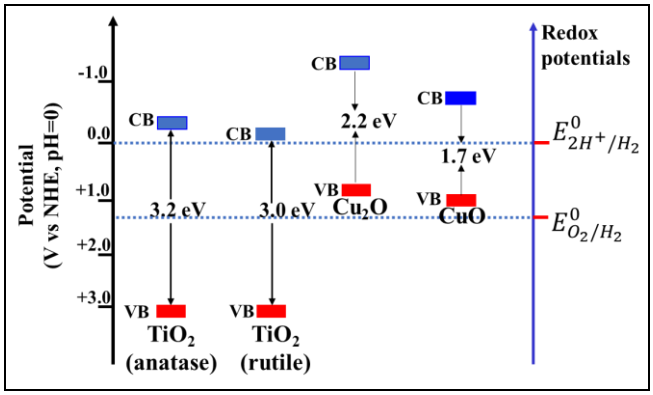

Fig 1: The position of the band edges of some semiconductors and the standard levels of hydrogen production and water oxidation at pH = 0 [5].

Although TiO_2 is a preferred candidate for H_2 production, its photocatalytic hydrogen generation efficiency is not high due to some of the main following reasons: *i)* the fast recombination rate of the photogenerated electron–hole pairs would also decrease the photocatalytic water splitting to hydrogen production performance*; ii)* The water decomposition reaction into hydrogen and oxygen has a large positive Gibbs free energy (ΔG = 237 kJ/mol) led to the recombination of hydrogen and oxygen into water reaction easily proceeds [3], and *iii)* the large optical bandgap of TiO_2 (3.0 - 3.2 eV) led to TiO_2 can only be activated by UV light (only *5%* of the solar radiation in the solar spectrum). Loading of transition metals and its oxides (Ag, Pt, CuO, Cu_2O,) is an effective method to overcome these drawbacks. The transition metals with suitable work-

Function can prevent the recombination of electron–hole pairs, thus the photocatalytic activity of TiO_2 would improve. Compared to other metals, copper oxide species (CuO, Cu_2O) are one of the promising materials due to its low cost, abundant resources, and high photocatalytic hydrogen production performance. Specifically, Cu_2O is a simple metal oxide semiconductor with low bandgap energy 2.0 ÷ 2.2 eV. Their CB edge of -1.2 V (versus NHE, pH=0) is higher than that of TiO_2 (- 0.3 V versus NHE, pH=0) and the VB edge of Cu_2O (+ 1.0 versus NHE, pH = 0) is lower than that of TiO_2 (+ 2.8 V versus NHE, pH =0). Thus, the photogenerated electrons can transfer from CB of Cu_2O to that of TiO_2, and the photogenerated holes can jump into VB of TiO_2 to that of Cu_2O under irradiation with a suitable light source. As a result, the photogenerated electrons-holes pairs are separated from each other, reducing the recombination probability and increasing the lifetimes of the charge carriers [6].

Recently, various researchers have been reported the efficiency photocatalytic H_2 generation of Cu_2O/TiO_2 composites. Lalitha *et al*. reported that the photocatalytic H_2 generation of water and water: glycerol mixtures over CuO/TiO_2 and Cu_2O/TiO_2 photocatalyst significantly enhanced. The maximum of hydrogen production was ~ 265 and ~290 µmol h^- for 2 wt% CuO/TiO_2 and Cu_2O/TiO_2 catalysts in pure water, respectively [7]. Hinojosa-Reyes *et al*. reported that the hydrogen production of Cu_2O-TiO_2 photocatalysts was prepared by the sol-gel method. The results showcased that the copper concentration and annealed temperatures played a significant role in the hydrogen photocatalytic production rate [8]. Another report, it was proved that the effects of Cu_2O morphology were responsible for enhancing the photocatalytic hydrogen generation, the results indicated that TiO_2 film/Cu_2O with microgrid structures exhibited the higher efficiency in hydrogen production than the TiO_2 film/Cu_2O film owing to the existence of Ti^{3+} states and the easy contact of H^+ ions with electrons to H_2 gas in microgrid structures, leading to enhanced the photocatalytic H_2 performance in TiO_2 film/Cu_2O microgrid [9].

For the aforementioned reasons, the purpose of this work is to investigate the effect of the crystal structure of catalysts on the H_2 generation performance under UV irradiation of Cu_2O/TiO_2 composite by changing the annealing temperature. In this study, the Cu_2O/TiO_2 composite is fabricated by the hydrothermal and impregnation method. The enhancement mechanism of the photocatalytic H_2 production in this report will be explained and provided in detail. These results supply an insight into the role of crystal structure for enhancing practice applications as clean energy production.

2. Materials and Methods

2.1. Materials preparation

TiO_2 nanotube structures were fabricated by the hydrothermal technique. First, 4.2 g of TiO_2 powder was dispersed in 120 ml of 10 M NaOH aqueous solution by the magnetic stirrer for 4 hours at 50ºC; the TiO_2 + NaOH suspension was then heated at 130ºC for 22 hours in an autoclave. The white precipitates were gathered by centrifugation. After the centrifugation process, the white product was washed with distilled water until pH ~ 9, then 2 M HNO_3 acid was then slowly added to the distilled water until pH 7. Next, the white powder washed again with distilled water at 80ºC to remove the residue of sodium. Finally, this product was annealed at the various annealing temperature for 4 hours [10].

Cu_2O/TiO_2 was prepared by using the impregnation method by $Cu(NO_3)_2.3H_2O$ and TiO_2 nanotubes. First, 0.2 g TNTs was dispersed into $Cu(NO_3)_2.3H_2O$ aqueous solution (~ 50 mL with the content of Cu is 1.5 wt%), and constantly stirred for 8 hours at 80°C. Then, the sample was dried in air at 100°C overnight to evaporate fully the excess water out. The final product is a blue powder mixture. Finally, the samples are annealed at various temperatures (300ºC, 400ºC, 500ºC, 600ºC, and 700ºC) in the air for 2 hours with the heating and cooling rate of 5ºC min^{-1}. The process of fabrication of Cu_2O/TiO_2 is shown in Fig 2.

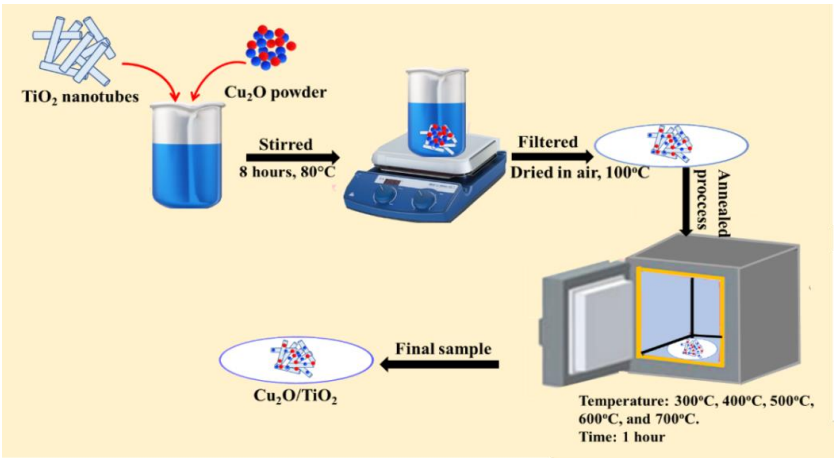

Fig 2: The fabricating process of Cu_2O/TiO_2 samples.

2.2. Characterization techniques

The crystalline phase of the nanotubes was investigated by Bruker D8 ADVANCE X-ray diffractometer (XRD) with =0.15406 nm. The Diffuse Reflectance UV–visible spectra were recorded on a UV-vis spectrophotometer (JASCO – V670) in the wavelength range 300 – 700 nm with a scan rate of 400 nm.min^{-1}. The chemical composition of the Cu_2O/TiO_2 sample was analyzed by an energy dispersive X-ray spectrometer (EDX). The morphology of TiO_2 modified Cu_2O samples was characterized by transmission electron microscopy (TEM, JEM−1400) operated at 100 kV. Photoluminescence (PL) emission spectra were analyzed

with a fluorescence spectrophotometer (Horiba iHR320) using 325 nm as the excitation source at room temperature. All the characterizations were carried out at room temperature.

Hydrogen performance tests: Photocatalytic H_2 production reactions were carried out under UV light and recorded by using an off-line HP-5890 gas chromatograph equipped with a thermal conductivity detector (TCD). Firstly, ~ 5 mg of the Cu_2O/TiO_2 powder was dispersed in 50 mL of 5 vol. % glycerol solution with continuous stirring. Then, the mixture is irradiated by UV light, and the evolved gaseous products were collected in the TCD system.

3. Results and Discussions

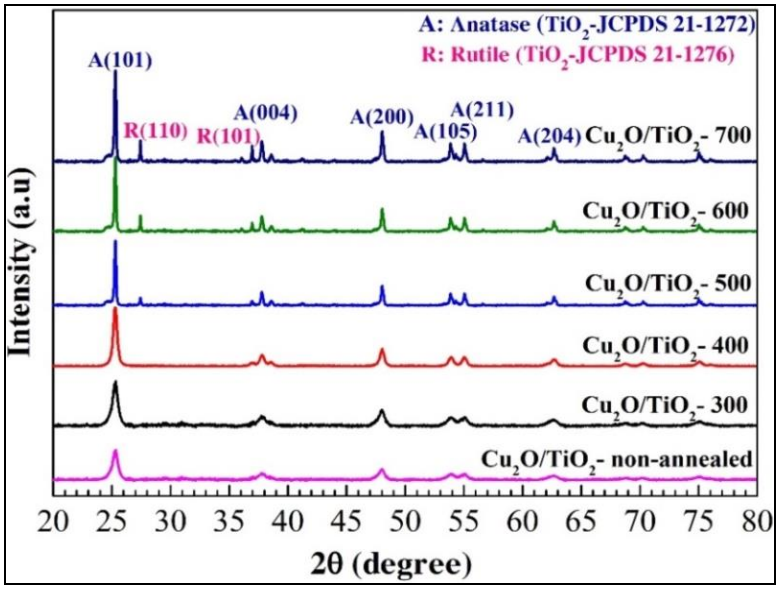

Fig 3: The XRD pattern of Cu_2O/TiO_2 annealed samples at the different temperatures.

The phase composition of Cu_2O/TiO_2 samples annealed at different temperatures was determined by XRD in Fig 3. We can see that the crystalline of samples increases with an increase in annealing treatment. This result reveals that the Cu_2O/TiO_2 annealed samples present peak characterizes of TiO_2 (JCPDS card no. 21-1272 and 21-1726), and there are only anatase diffraction peaks for samples annealed at 300ºC and 400ºC. The rutile peak starts appearing at 2θ = 27.47º, 35.89º which corresponds to (110), (101) plane in the structure of TiO_2 when annealing times are raised to 600ºC - 700ºC, and the rutile peak intensity increase with an increase in annealing temperature. The content of anatase and rutile phase is calculated by using equation [11]:

$$f = \frac{1}{1 + 1.265\left(\frac{I_R}{I_A}\right)}$$

Where f is the ratio of anatase in the mixture, I_A and I_R are intensities of anatase (101) and rutile (110) diffraction peaks. It observes that the content of anatase - rutile phase is 100% (A) - 0.00% (R) for Cu_2O/TiO_2 at 300ºC and 400ºC, while this composition are 82.30% (A) - 17.70% (R), 78.27 %(A) - 21.73 % (R), 71.16% (A) - 28.84% (R) at 500ºC, 600ºC, and 700ºC, respectively (Table 1). This implies that the anatase phase is transformed into the rutile phase in the heat treatment process, and the content of the rutile phase increases with an increase in annealing temperature. In addition, there is no peak of Cu or their oxide species (CuO, Cu_2O) is observed in XRD analysis. This result proved that Cu or their oxide species only exist on the surface of TiO_2 nanotubes. Indeed, the ion diameters of Ti^{4+} are about 74.5 pm (~ 0.0745 nm), which is smaller than that of Cu^{2+} is about 87 pm (0.087 nm) [6,12] which suggests that it is impossible for Cu^{2+} ion could replace Ti^{4+} ion at the crystal lattice site. For the influence of the annealing temperature on the average crystallite size, we can see from Fig 6 that when the annealing temperature increased, the peak intensity was higher, indicating that an increase in crystallite size and crystallinity at from 500°C to 700°C are observed. As shown in Table 1, the average crystallite size of samples was found to be from ~ 9.36 to ~ 36.46 nm corresponding to an increase in the annealing temperature from 300ºC to 700ºC, respectively. The result also indicates that the change of average crystallite size is due to the expanded regions of the grain boundaries since the temperature rises to lead to the presence of agglomeration particles during heating treatment. This behavior of the average crystallite size is in agreement with previous works [13,14]. This means that the increase of the annealing temperature results in not only larger particles of samples but also the effect of the phase transition of TiO_2.

Table 1: The change of the average crystal size and crystal composition anatase - rutile phase of Cu_2O/TiO_2 annealed at different temperature.

Samples	Average crystal size (nm)	I_A (101 Anatase)	I_B (110 Rutile)	% Anatase	% Rutile
Cu_2O/TiO_2-300	9.36 ± 1	2513.06	0	100.00	0.00
Cu_2O/TiO_2-400	16.56 ± 1	3316.78	0	100.00	0.00
Cu_2O/TiO_2-500	24.51 ± 1	3013.52	488.23	82.30	17.70
Cu_2O/TiO_2-600	31.61 ± 1	4097.79	899.22	78.27	21.73
Cu_2O/TiO_2-700	36.46 ± 1	5067.01	1586.95	71.16	28.84

Fig. 4 exhibits the Raman spectra analysis of the Cu_2O/TiO_2-500 samples annealed at 500 ºC. This result

revealed the existence of TiO_2 characteristic phases. The Raman peaks at 144, 398, 513, 637 cm^{-1} denote $E_g(1)$, $B_{1g}(1)$, $A_{1g}(1)+ B_{1g}(2)$, $E_g(3)$ standard modes of TiO_2 [15,16]. The symmetric stretching vibration of O – Ti – O bond is observed at 144 and 398 cm^{-1} associated with E_g anatase mode, the symmetric and anti-symmetric bending vibration of O-Ti-O bond is associated with B_{1g} (1) and $A_{1g}(1)$ modes. However, no peak characteristic related to the phonon frequencies of the crystalline Cu_2O has detected in this curve. The lack of 146 cm^{-1} and 219 cm^{-1} means that Cu_2O is not present in Cu_2O/TiO_2 heterojunction structure [17, 18]. This result is already an agreement with XRD analysis.

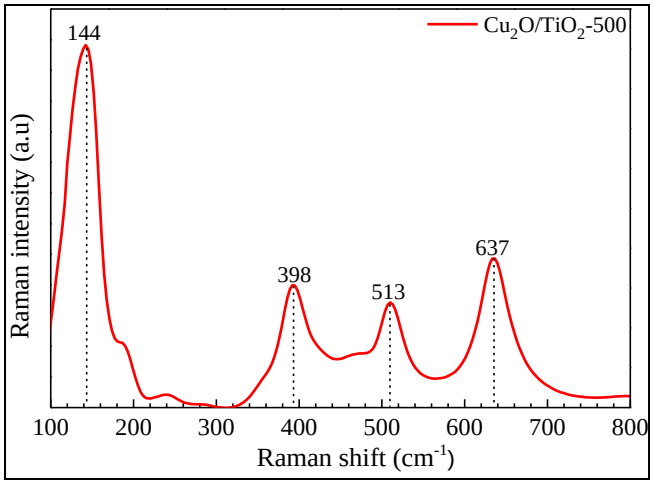

Fig 4: Raman spectrum analysis of Cu_2O/TiO_2 sample annealed at 500ºC.

The UV-vis diffuse reflectance spectra of TiO_2 and Cu_2O/TiO_2 samples are shown in Fig. 5. The corresponding band gap energy values (E_g) are calculated by using the Kubelka-Munk equation (calculated from the formula $\lambda = 1239.8/E_g$), and plotted by the Tauc method as shown in Fig. 5 [19,20]. For the pure TiO_2-500, strong absorption of the ultraviolet (UV) light is observed at about 380 nm corresponding to the bandgap energy of 3.25 eV. This absorption band in the UV region of the pure TiO_2 can be attributed to the bandgap excitation of anatase TiO_2 related to the band to the band transition [21]. The absorption in the visible region (from 400 to 500 nm) for Cu_2O/TiO_2 samples is observed in Fig. 5. This result revealed that the Appearance of Cu_2O nanoparticle on the TiO_2 surface leads to reducing the bandgap energy of the heterojunction structure. Besides, the raise of annealing temperature pushes the UV-Vis diffuse reflectance spectra to the visible region, corresponding to the reduction of the energy bandgap (E_g). As seen in Fig. 5, the absorbance wavelength of samples annealed at 300ºC, 400ºC, 500°C, 600°C, and 700°C was 413 nm, 440 nm, 450 nm, 460 nm, and 591 nm, respectively, corresponding to the bandgap energy of 3.0 eV, 2.82 eV, 2.75 eV, 2.7 eV, and 2.1 eV, respectively. These results indicated that after being increased the annealing temperature, the energy of bandgap declines that can be governed by the partial crystallization of the samples, and the crystallization of the samples.

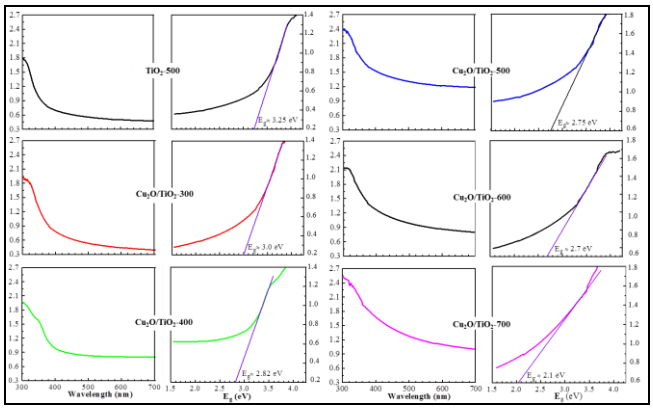

Fig 5: The UV-visible absorption spectra and Tauc plots used to determine E_g (b) of TiO_2 and Cu_2O/TiO_2 samples.

Fig. 6 displays the TEM image of Cu_2O/TiO_2 samples. It is observed that the surface morphology of sample shows varies remarkably with the change of annealing temperatures. There are no great changes in the diameter and tube at 300ºC and 400ºC (Fig. 6 (a) and Fig. 6 (b)). However, the tube structure is broken and the length of the tube is shortened at 500ºC. When the temperature rises to 600ºC and 700ºC, the tube is almost destroyed and transformed into the particle structure (Fig. 6 (c) and Fig. 6 (d)). The same phenomena are fully consistent with the model of the structure growth of TiO_2 nanotubes and the anatase-rutile phase transformation at a high temperature of TiO_2 in the previous section.

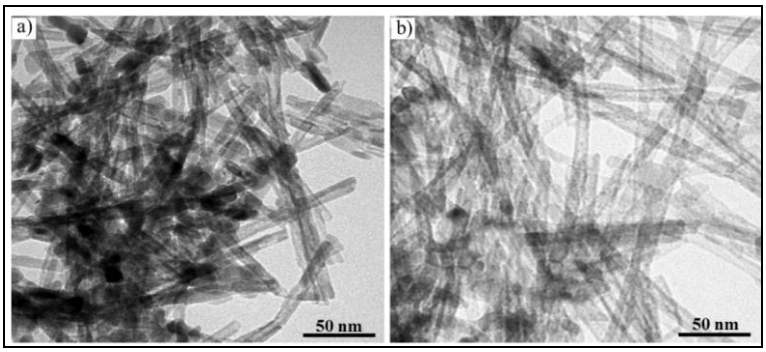

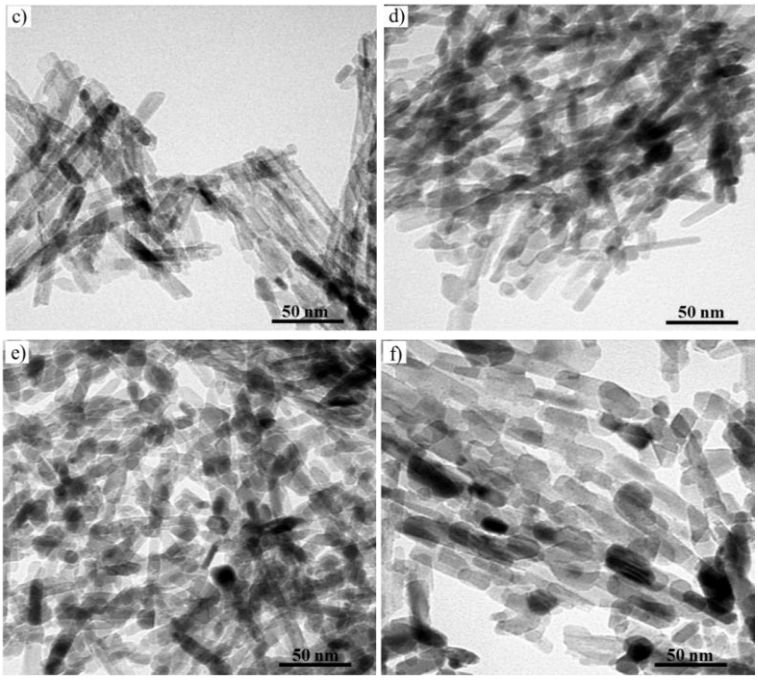

Fig 6: TEM images of Cu_2O/TiO_2 structure annealed at (a) non-annealed, (b) 300ºC, (c) 400ºC, (d) 500ºC, (e) 600ºC, and (f) 700ºC.

The photoluminescence emission (PL) spectra of Cu_2O/TiO_2 in wavelength at 350-600 nm are shown in Fig. 7. It can be seen that the PL shape and their intensity change significantly with the increasing annealing temperature, while, their intensity decreases linearly. At 300ºC, 400ºC, and 500ºC, the curve is similar. At 600ºC and 700ºC, they have significantly differences. The Gaussian function is used to analyze the PL spectra of samples annealed at 300ºC, 500ºC, and 700ºC (Fig. 7 (b,c,d)). The PL peak at 385 nm describes the band−band phenomenon emission with the energy approximately equal to the bandgap energy (3.2 eV) of the TiO_2 anatase phase [22]. The PL peak at 420 nm is dominated by the near bandgap emission from the rutile phase while two peaks at 490 nm, 530 nm can be attributed to the excitonic transitions from TiO_2 intrinsic defects as the self-trapped exciton and the surface defect states of oxygen vacancies (V_o) [23,24]. According to the photoluminescence spectroscopy theory, PL spectra is also proven to be a good tool for checking the photophysical properties of the material including the efficiency of charge carrier trapping and recombination of electron - holes pairs on the surface of the photocatalyst [25]. In addition, the intensity of PL emission that is correlated to the e^--h^+ recombination rate in semiconductor, the sample with a lower emission intensity could be indicated that it has a lower electron-hole recombination rate that would result in higher photocatalytic activity as well as hydrogen generation performance [26]. This result implies that the PL emission intensity significantly reduced with the increasing annealing temperature. The PL emission intensity at 500ºC, 600ºC, and 700ºC are lower than the sample at 300ºC, 400ºC, and the lowest intensity is at 700ºC. This suggests that the annealing process might be responsible for improving the separation of the photo-generated e^--h^+ pairs and suppressing recombination in the Cu_2O/TiO_2 heterojunction structure. From the above discussion, it could be expected that samples at 500ºC-700ºC possess high photocatalytic hydrogen generation ability compared to 300ºC and 400ºC.

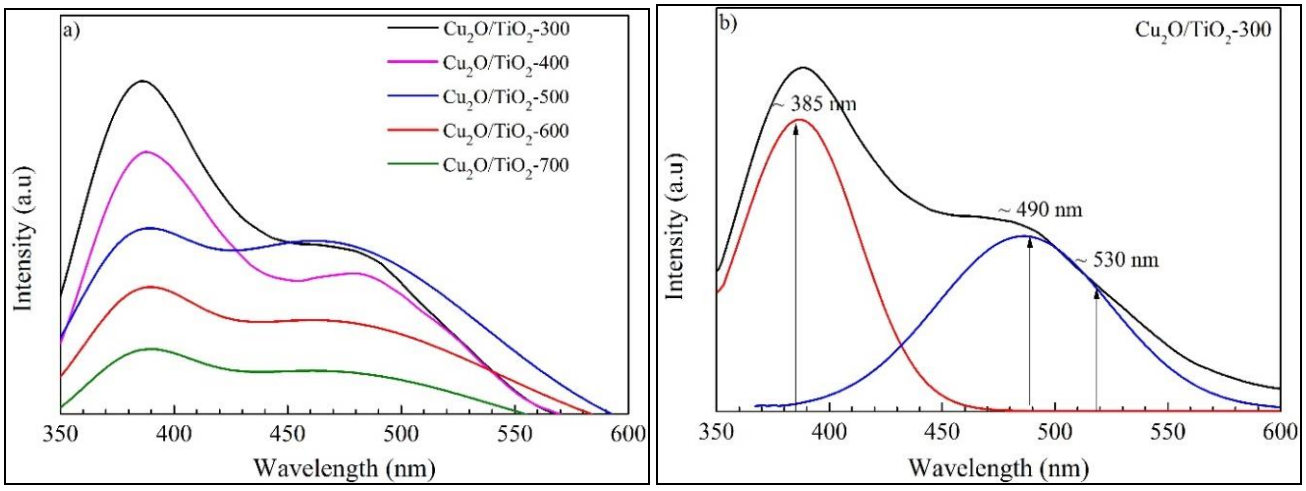

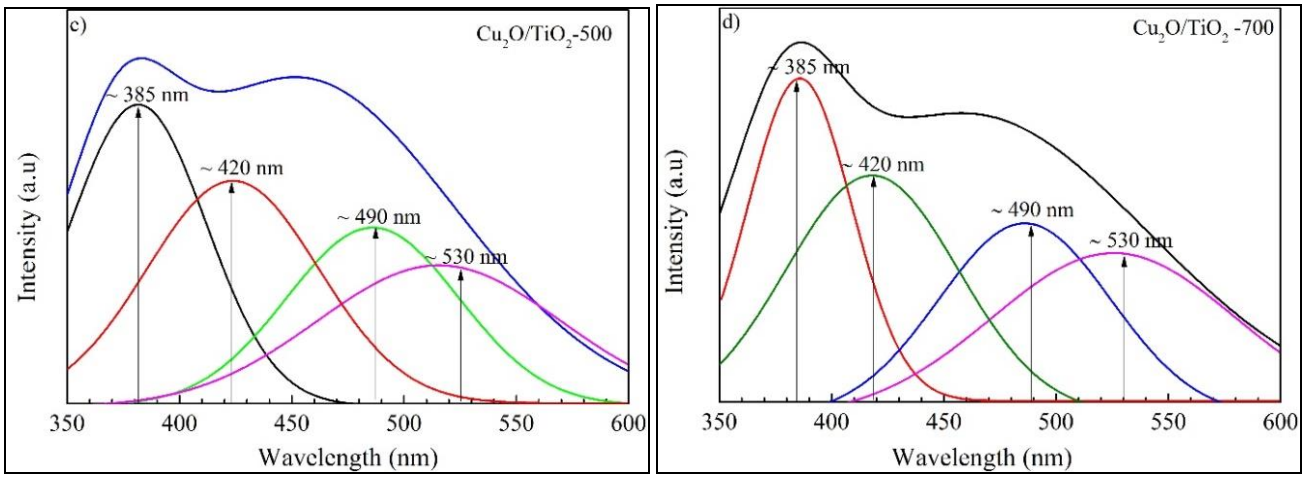

Fig 7: The photoluminescence emission (PL) spectra of Cu_2O/TiO_2 annealed at different temperatures (a), and the deconvolution PL curve, respectively (b,c,d).

Photocatalytic hydrogen evolution reactions were carried out by UV irradiation with Hg lamp, and the total amount of hydrogen produced is plotted as a function of irradiation time. The hydrogen production of TiO_2 nanotubes and Cu_2O/TiO_2 samples is shown in Fig. 8. Compared to TiO_2-500 nanotubes, Cu_2O/TiO_2 samples exhibit a higher photocatalytic activity for hydrogen production. In addition, the annealing temperature affects the performance of photocatalytic hydrogen generation of Cu_2O/TiO_2 samples. The rate of hydrogen evolution increased slowly within the first hour, then increased a steady and *g*radually faster, which may be due to the presence of Cu species nanocluster on the wall of TiO_2 leading to enhancing the photocatalytic activity of Cu_2O/TiO_2 heterojunction structure.

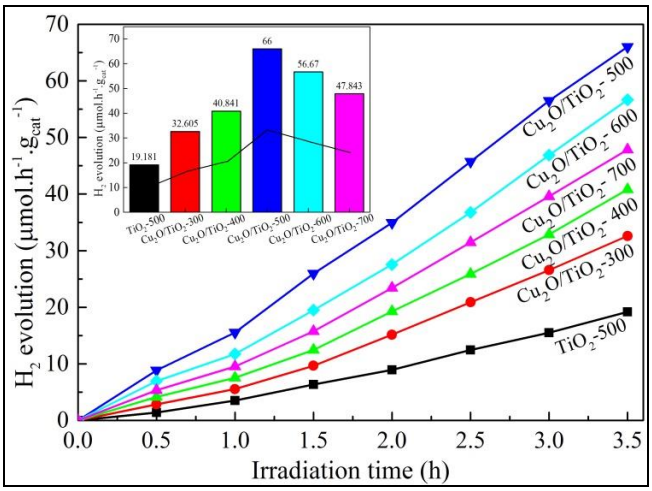

Fig 8: Photocatalytic hydrogen production rate collected for TiO_2 nanotubes and Cu_2O/TiO_2 samples under UV irradiation.

The hydrogen production rate increases with the increase in annealing temperature from 300ºC - 500ºC, and then decreased at 600ºC and 700ºC. At 300ºC and 400ºC, the hydrogen production rate increased from 32.60 $\mu mol.h^{-1}.gcat.^{-1}$ to 40.84 $\mu mol.h^{-1}.gcat.^{-1}$, respectively. The hydrogen performance reaches a maximum at 500ºC with 66.03 $\mu mol.h^{-1}.gcat.^{-1}$. At 600ºC and 700ºC, the hydrogen volume production rate drops to 56.67 $\mu mol.h^{-1}.gcat.^{-1}$ and 47.83 $\mu mol.h^{-1}.gcat.^{-1}$. This means that the hydrogen production efficiency is significantly affected by the change of the phase composition, grain size, and agglomerate size due to annealing temperature. It is seen from Table 1, the predominant rutile phase at 600°C and 700ºC with the % rutile composition is about 21.73 and 28.84, respectively, and it was higher than other samples. This result notes that the composition of the rutile phase notably affects the H_2 evolution. The lower rutile phase content appeared at 500ºC is more active in the photocatalytic production of hydrogen. The same phenomena are observed by other reported. Indeed, Li *et al*. reported that the appearance of the rutile phase in the crystal structure of TiO_2 notably effected H_2 evolution and this nanoparticle system of Cu_2O coupled with TiO_2 nanoparticles exhibited a lower rate of H_2 production compared with Cu_2O nanoparticles incorporated TiO_2 nanotubes [21]. The Cu_2O/TiO_2-500 structure demonstrates the highest rate of H_2 production 66.03 $mmol.h^{-1}.gcat.^{-1}$ with an apparent quantum efficiency of 10.8% at 365 nm [22]. Therefore, in this experiment, the annealing temperatures of 500°C are effectively suitable for photocatalytic H_2 production enhancement of Cu_2O/TiO_2 heterojunction structure.

The enhancement in the hydrogen production performance of Cu_2O/TiO_2 heterojunction structure is explained by reaction equations (eq) (1) - (5), and the photogenerated charge transfer mechanism in the Cu_2O/TiO_2 heterojunction structure in Fig. 9 as follows [27-29]:

$$Ti_2O + h\nu \rightarrow Ti_2O\,(e^-) + Ti_2O\,(h^+) \quad (1)$$

$$Cu_2O + h\nu \rightarrow Cu_2O(e^-) + Cu_2O(h^+) \quad (2)$$
$$2e^- + 2H_2O \rightarrow H_2 + 2OH^- \quad (3)$$
$$h^+ + H_2O \rightarrow {}^*OH + H^+ \quad (4)$$
$$2e^- + 2H^+ \rightarrow H_2 \quad (5)$$

When the Cu_2O/TiO_2 heterojunction structure is excited by UV irradiation, the photo-generated charge (electron -hole pairs) are generated as eq (1) and eq (2). Because the conduction band (CB) edge of Cu_2O is more negative than that of TiO_2 (Fig. 1), the electrons on the CB of Cu_2O can be easily transferred to that of TiO_2; meanwhile, the holes on the VB of TiO_2 can be easily transferred to that of Cu_2O. Hence the holes density in the VB of TiO_2 is drained, whereas, the holes density is enhanced in that of Cu_2O and form the holes center in Cu_2O (Fig. 9). Therefore, e^- transfers from Cu_2O to TiO_2 and h^+ transfers from TiO_2 to Cu_2O can effectively separate the photogenerated charge ($e^- - h^+$) as well as preventing the recombination of them that can improve photocatalytic hydrogen generation ability. Due to the high potential energy, the e^- accumulated in the CB of TiO_2 can reduce H^+ ion to form H_2 gas (eq (3)). On the other hand, e^- can react with H^+ ion produced by dehydration reaction in eq (4) to produce H_2 in eq (5). Thus, the photocatalytic hydrogen production activity of Cu_2O/TiO_2 structure is significantly improved due to the presence of Cu_2O on the wall of TiO_2 nanotubes.

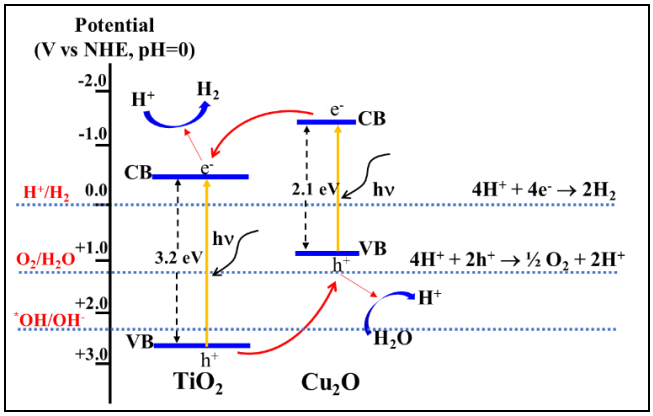

Fig 9: The photogenerated charge transfer mechanism in the Cu_2O/TiO_2 heterojunction structure under UV irradiation.

4. Conclusions

In this work, we have synthesized the Cu_2O/TiO_2 heterojunction structure by the hydrothermal and impregnation method. The obtained result demonstrates that the production efficiency of H_2 of Cu_2O/TiO_2 heterojunction structure can be significantly affected by annealing temperature (phase composition, crystalline, grain size, and agglomerate size). The hydrogen production performance of Cu_2O/TiO_2 heterojunction structure increases at 300°C-500°C and decreases at 600°C - 700°C. The highest quantum efficiency obtained was about 10.8% (66.03 $\mu mol.h^{-1}.g_{cat}^{-1}$) is for Cu_2O/TiO_2-500 sample with about 24.5 nm particle size, 82.30% (A) - 17.70% (R) phase composition, the smallest bandgap energy (E_g ~ 2.4 eV). In addition, we notice that the photogenerated charge transfer mechanism of different semiconductors is also one of the influencing factors to the production efficiency of H_2.

5. Acknowledgements

This research is supported by project the SPD2018.01.23.

6. References

1. Zoulias E, Varkaraki E, Lymberopoulos N, Christodoulou C N, & Karagiorgis G N. A review on water electrolysis. Tcjst. 2004; 4(2): 41-71.
2. Van de Krol R, & Grätzel M. Photoelectrochemical hydrogen production (Vol. 90). New York: Springer, 2012.
3. Liao CH, Huang CW, & Wu J. Hydrogen production from semiconductor-based photocatalysis via water splitting. Catalysts. 2012; 2(4):490-516.
4. Kudo A, & Miseki Y. Heterogeneous photocatalyst materials for water splitting. Chemical Society Reviews. 2009; 38(1):253-278.
5. Pan H, Zhu S, Lou X, Mao L, Lin J, Tian F, & Zhang D. Graphene-based photocatalysts for oxygen evolution from water. RSC advances. 2015; 5(9):6543-6552.
6. Janczarek M, Kowalska E. On the origin of enhanced photocatalytic activity of copper-modified titania in the oxidative reaction systems. Catalysts. 2017; 7(11):317.
7. Lalitha K, Sadanandam G, Kumari VD, Subrahmanyam M, Sreedhar B, & Hebalkar N Y. Highly stabilized and finely dispersed Cu_2O/TiO_2: a promising visible sensitive photocatalyst for continuous production of hydrogen from glycerol: water mixtures. The Journal of Physical Chemistry C. 2010; 114(50):22181-22189.
8. Hinojosa-Reyes M, Camposeco-Solís R, Zanella R, & González V R. Hydrogen production by tailoring the brookite and Cu_2O ratio of sol-gel Cu-TiO_2 photocatalysts. Chemosphere, 2017; 184:992-1002.
9. Zhu L, Zhang J, Chen Z, Liu K, & Gao H. Effect of Cu_2O morphology on photocatalytic hydrogen generation and chemical stability of TiO_2/Cu_2O composite. Journal of nanoscience and nanotechnology. 2013; 13(7):5104-5108.
10. Le TNT, Ton NQT, Tran VM, Dang Nam N, Vu TH T. TiO_2 nanotubes with different Ag loading to enhance visible-light photocatalytic activity. Journal of Nanomaterials, 2017.
11. Klug HP. Quantitative analysis of powder mixtures with Geiger-Counter spectrometer. Analytical Chemistry. 1953; 25(5):704-708.
12. Yan H, Zhao T, Li X, & Hun C. Synthesis of Cu-doped nano-TiO_2 by detonation method. Ceramics International. 2015; 41(10):14204-14211.
13. Sun Y, Yan K, Wang G, Guo W, & Ma T. Effect of annealing temperature on the hydrogen production of TiO_2 nanotube arrays in a two-compartment photoelectrochemical cell. The Journal of Physical Chemistry C. 2011; 115(26):12844-12849.
14. Mathur S, Arya M, Jain R, Sharma SK. Effect of annealing temperature on structural, electrical and optical properties of TiO_2 nanopowder. Journal of Nanostructures. 2017; 7(2):121-126.
15. Priyanka KP, Revathy VR, Rosmin P, Thrivedu B, Elsa KM, Nimmymol J, Varghese T, *et al*. Influence of La doping on structural and optical properties of TiO_2 nanocrystals. Materials Characterization. 2016; 113:144-151.
16. Mazza T, Barborini E, Piseri P, Milani P, Cattaneo D, Bassi AL, Ducati C, *et al*. Raman spectroscopy characterization of TiO_2 rutile nanocrystals. Physical

Review B. 2007; 75(4):045416.
17. Tounsi N, Barhoumi A, Akkari FC, Kanzari M, Guermazi H, Guermazi S, *et al*. Structural and optical characterization of copper oxide composite thin films elaborated by GLAD technique. Vacuum. 2015; 121:9-17.
18. Deng Y, Handoko A D, Du Y, Xi S, Yeo BS. In situ Raman spectroscopy of copper and copper oxide surfaces during electrochemical oxygen evolution reaction: identification of CuIII oxides as catalytically active species. ACS Catalysis. 2016; 6(4):2473-2481.
19. Xu X, Gao Z, Cui Z, Liang Y, Li Z, Zhu S, Ma J, *et al*. Synthesis of Cu_2O octadecahedron/TiO_2 quantum dot heterojunctions with high visible light photocatalytic activity and high stability. ACS applied materials & interfaces. 2016; 8(1):91-101.
20. Tamiolakis I, Papadas IT, Spyridopoulos KC, Armatas GS. Mesoporous assembled structures of Cu_2O and TiO_2 nanoparticles for highly efficient photocatalytic hydrogen generation from water. RSC advances. 2016; 6(60):54848-54855.
21. Li Y, Wang B, Liu S, Duan X, & Hu Z. Synthesis and characterization of Cu_2O/TiO_2 photocatalysts for H_2 evolution from aqueous solution with different scavengers. Applied Surface Science. 2015; 324:736-744.
22. Suisalu A, Aarik J, Mändar H, Sildos I. Spectroscopic study of nanocrystalline TiO_2 thin films grown by atomic layer deposition. Thin Solid Films. 1998; 336(1-2):295-298.
23. Lei Y, Zhang LD, Meng GW, Li GH, Zhang XY, Liang CH, Wang SX. Preparation and photoluminescence of highly ordered TiO_2 nanowire arrays. Applied physics letters. 2001; 78(8):1125-1127.
24. Ansari SA, Cho MH. Highly visible light responsive, narrow band gap TiO_2 nanoparticles modified by elemental red phosphorus for photocatalysis and photoelectrochemical applications. Scientific reports. 2016; 6(1):1-10.
25. Hurum DC, Agrios AG, Gray KA, Rajh T, Thurnauer MC. Explaining the enhanced photocatalytic activity of Degussa P25 7mixed-phase TiO_2 using EPR. The Journal of Physical Chemistry B. 2003; 107(19):4545-4549.
26. Gupta K, Singh RP. Anjana Pandey Photocatalytic antibacterial performance of TiO_2 and Ag-doped TiO_2 against S. aureus. P. aeruginosa and E. coli. Beilstein J. Nanotechnol. 2013; 4:345-351.
27. Zhang J, Wang Y, Yu C, Shu X, Jiang L, Cui J, Wu Y. Enhanced visible-light photoelectrochemical behaviour of heterojunction composite with Cu_2O nanoparticles-decorated TiO_2 nanotube arrays. New Journal of Chemistry. 2014; 38(10):4975-4984.
28. Xie Y, Ali G, Yoo SH, Cho SO. Sonication-assisted synthesis of CdS quantum-dot-sensitized TiO_2 nanotube arrays with enhanced photoelectrochemical and photocatalytic activity. ACS applied materials & interfaces. 2010; 2(10):2910-2914.
29. Fu J, Cao S, Yu J. Dual Z-scheme charge transfer in TiO_2–Ag–Cu_2O composite for enhanced photocatalytic hydrogen generation. Journal of Materiomics. 2015; 1(2):124-133.